

# Wetting in Asymmetric Quasi-2D Systems

Ziad Khattari,<sup>†</sup> Peter Heinig,<sup>†</sup> Stefan Wurlitzer,<sup>†</sup> Paul Steffen,<sup>†</sup>  
Mathias Lösche,<sup>‡</sup> and Thomas M. Fischer<sup>\*,†</sup>

Max Planck Institute of Colloids and Interfaces, Am Mühlenberg 1, 14476 Golm, Germany,  
and University of Leipzig, Institute of Experimental Physics I, Linnéstrasse 5,  
04103 Leipzig, Germany

Received October 8, 2001. In Final Form: December 7, 2001

The effect of electrostatic dipole interactions on the wetting behavior of two-dimensional droplets, approximated by circular segment shapes with contact angle  $\alpha$ , is investigated.  $\alpha$  depends on the geometric structure far away from the three-phase contact point. We theoretically find metastable  $\alpha$  values associated with transitions from complete wetting to partial dewetting, triggered by minute changes of the film area, the surface potential of the coexisting phases, or their line tensions. The predictions are confirmed experimentally in a Langmuir monolayer model system. The wetting instability may influence intramembrane biochemical reactions between protein species dissolved in coexisting phases via the length of the contact line between the phases, the only region where chemical reactions between the species are possible.

## Introduction

The wetting properties<sup>1–3</sup> of liquids are characterized by the contact angle  $\alpha$ , a materials parameter in three-dimensional (3D) systems.<sup>4</sup> The physics of wetting within systems of lower dimensionality, such as molecularly thin dipolar interface films,<sup>5</sup> is different because of long-range correlations between collinearly oriented dipole moments, which exist not only in solid phases, as in ferroelectrics in 3D, but also in laterally disordered—fluid or even gaseous—phases because of the symmetry break inferred by the interface.<sup>6</sup> Here we show theoretically and demonstrate experimentally using a Langmuir monolayer<sup>7</sup> that the shape of circular segment droplets, described by their contact angle  $\alpha$ , depends on the droplet area and film structure far away from the three-phase contact point. We find metastable  $\alpha$  values associated with transitions from complete wetting to partial dewetting, triggered by minute changes of the film area, the surface potential of the coexisting phases, or their mutual line tensions. These findings bear implications for the regulation of biomembrane functions, since the phenomenon may influence intramembrane biochemical reactions<sup>8–10</sup> between protein species dissolved in coexisting phases.<sup>11</sup> A change in contact angle will result in a different length of the contact lines between two of the three phases. The contact lines are the regions where chemical reaction between species dissolved in the phases might occur and where aggregation of material might result in growth of one of the phases at

the expense of the other. Therefore, the length of the contact line will have an effect on the rate constant of such reactions.

## Theoretical Background

Langmuir monolayers<sup>7</sup> as well as biological cell membranes are quasi-2D systems in which effective dipole moments, that is, the sum of real and image charges, associated with the constituent, lipid or protein molecules, are axially oriented across an interface.<sup>8</sup> While mesoscopic phase separation in Langmuir monolayers is well established,<sup>12</sup> for biological membranes it has only recently been shown for polarized cells that the lateral structure is heterogeneous on the nanoscopic scale,<sup>11</sup> and at least two phases of different lipid composition coexist. The structure of such phases is controlled by the competition of long-range dipolar interactions between the constituent lipids and the line tension between the coexisting phases.<sup>5</sup> Coexisting lipid phases ( $i = 1, 2, 3, \dots$ ) in a molecular layer system that mimics a biomembrane are characterized by distinct homogeneous dipole moment densities  $\mu_i$ .<sup>13</sup> In continuum models aiming at a quantitative description of their properties, dipole–dipole interactions are cut off at distances  $\Delta < 6 \text{ \AA}$  to account for the nonhomogeneous structure on the molecular scale<sup>5</sup> ( $\Delta$  is approximately the lateral spacing between the lipids; only the order of magnitude of  $\Delta$  matters, because in all relevant equations  $\Delta$  enters as a logarithmic correction factor). Associated with each phase boundary within such a quasi-2D system is a line tension  $\lambda_{ij}$  that accounts for the excess energy per unit length. For a general heterogeneous distribution of lipid phases, the free energy reads

$$F = \sum_{ij} \frac{\mu_i \mu_j}{2} \int_{A_i} \int_{A_j} \frac{dA_i dA_j}{(|\mathbf{r} - \mathbf{r}'|^2 + \Delta^2)^{3/2}} + \sum_{ij} \lambda_{ij} \int_{\partial A_i \cap \partial A_j} ds \quad (1)$$

where  $\partial A_i \cap \partial A_j$  denotes the boundaries between phases

(12) Lösche, M.; Sackmann, E.; Möhwald, H. *Ber. Bunsen-Ges. Phys. Chem.* **1983**, *87*, 848–852.

(13) Dipole densities are measured in the units (pN)<sup>1/2</sup> and, in the case of Langmuir surface monolayers, defined as  $\mu_i = (\epsilon_0 \epsilon_w \epsilon_{\text{air}} / 2\pi (\epsilon_w + \epsilon_{\text{air}}))^{1/2} \Delta V_i$ , where  $\epsilon_0$  is the permittivity of vacuum,  $\epsilon_w$  ( $\epsilon_{\text{air}}$ ) is the relative permittivity of water (air), and  $\Delta V_i$  is the surface potential of phase  $i$ .

\* To whom correspondence should be addressed.

<sup>†</sup> Max Planck Institute of Colloids and Interfaces.

<sup>‡</sup> University of Leipzig.

(1) DeGennes, P. G. *Rev. Mod. Phys.* **1985**, *57*, 827–863.

(2) Pandit, R.; Fisher, M. E. *Phys. Rev. Lett.* **1983**, *51*, 1772–1775.

(3) Cahn, J. W. *J. Chem. Phys.* **1977**, *66*, 3667–3672.

(4) Young, T. *Philos. Trans. R. Soc. London* **1805**, *95*, 65–87.

(5) McConnell, H. M. *Annu. Rev. Phys. Chem.* **1991**, *42*, 171–195.

(6) Krüger, P.; Lösche, M. *Phys. Rev. E* **2000**, *62*, 7031–7043.

(7) Kaganer, V. M.; Möhwald, H.; Dutta, P. *Rev. Mod. Phys.* **2000**, *71*, 779–819.

(8) Babcock, G. T.; Wikström, M. *Nature* **1992**, *356*, 301–309.

(9) Lee, J.-D.; Kravchenko, V.; Kirkland, T. N.; Han, J.; Mackman, N.; Moriarty, A.; Leturcq, D.; Tobias, P. S.; Ulevitch, R. J. *Proc. Natl. Acad. Sci. U.S.A.* **1993**, *90*, 9930–9934.

(10) Hofmann, K. P.; Heck, M. Light-induced protein–protein interactions on the rod photoreceptor disc membrane. In *Biomembranes*; Lee, A. G., Ed.; JAI Press: 1996; Vol. 2A, pp 141–198.

(11) Rietveld, A.; Simons, K. *Biochim. Biophys. Acta* **1998**, *1376*, 467–479.

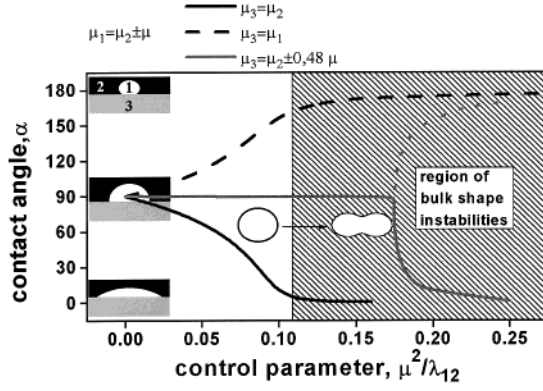


**Figure 1.** Theoretical prediction for the contact angle of a quasi-2D dipolar droplet (phase 1) of a reduced diameter,  $A^{1/2}/\Delta = 1000$  ( $A$ , area of the droplet;  $\Delta$ , electrostatic cutoff length), at an indifferent ( $S = -1$ ) supporting phase (phase 3) surrounded by gas (phase 2), plotted as a function of  $\mu^2/\lambda_{12}$ . Solid black line (case a):  $\mu_1$  differs from the other dipole moment densities by an excess dipole density  $\mu$ . Dashed black line (case b):  $\mu_2$  differs from  $\mu_1 = \mu_3$ . Gray lines (case c):  $\mu_1 = \mu_2 \pm \mu$  and  $\mu_3 = \mu_2 \pm 0.48\mu$ . Solid gray lines represent stable contact angles while dotted lines represent metastable solutions. The wetting (dewetting) transition occurs after a shape instability, where circular droplets in the bulk of phase 2 change their shapes toward elongated droplets. Similar behavior is observed as a function of  $A^{1/2}/\Delta$  for fixed  $\mu^2/\lambda_{12}$ . For simplicity, the theory is derived for a straight interface between phases 1 and 3, as depicted in the figure. In the experiments all interfaces are usually curved.

$i$  and  $j$ . The first term in eq 1 describes the electrostatic interaction between phases of different dipole density, and the second term describes contributions from the line tensions between the coexisting phases. The free energy (eq 1) has been successfully used to predict a rich variety of heterogeneous structures between two coexisting phases.<sup>5</sup> The most prominent effect of the dipolar energy term in eq 1 is to inhibit a macroscopic phase separation between two coexisting phases. Instead, a hexagonal or hexatic arrangement of mesoscopic domains of the minority phase with areas of the order  $\Delta^2 \exp(2\lambda_{ij}/(\mu_i - \mu_j)^2)$  is predicted theoretically and observed experimentally. For values of  $(\mu_i - \mu_j)^2/\lambda_{ij} < 0.3$ , as observed in many experiments on monolayers, the parameter  $\Delta^2/A$  is small ( $\Delta^2/A \ll 10^{-3}$ ).

We have analytically calculated the energy  $F$  (eq 1) of a particularly relevant 2D phase structure of three coexisting phases (*cf.* inset in Figure 1). The calculation (for details, see Appendices a–d) has been restricted to an arrangement of phases characterized by a sessile droplet of one phase (e.g., a fluid phase, denoted 1) connected to a second phase (gas phase or fluid II, denoted 2) via a circular segment and attached with its base to a third phase (an ordered phase, denoted 3). The total energy of this configuration depends on the dipole moment differences between the phases, the line tensions, and the droplet area,  $A$ . The calculation yields general properties of the thermodynamically stable phase morphology, in particular the contact angle  $\alpha$  describing the shape of the droplet. Within the framework of the theory a contact angle of the order  $\alpha \approx \Delta^2/A$  refers to a droplet with a thickness of the order of the spacing between the lipids and is the limiting contact angle where a continuum model makes sense. We will talk of complete wetting if  $\alpha \approx \Delta^2/A$ , of complete dewetting if  $\alpha \approx \pi - (\Delta/A^{1/2})^{1/2}$ , and of partial wetting/dewetting if  $\Delta^2/A \ll \alpha$  and  $\pi - \alpha \gg (\Delta/A^{1/2})^{1/2}$ . The definitions are appropriate for finite size droplets. In the thermodynamic limit,  $A \rightarrow \infty$ , they coincide with the usual

definitions, that is, complete wetting if  $\alpha = 0$ , complete dewetting if  $\alpha = \pi$ , and partial wetting/dewetting if  $0 < \alpha < \pi$ .

In a 3D system and in a 2D system with identical dipole densities  $\mu_i$ , the equilibrium contact angle is given by Young's equation,

$$\cos \alpha = S + 1 \quad (2)$$

where

$$S = (\lambda_{23} - \lambda_{13} - \lambda_{12})/\lambda_{12} \quad (3)$$

is a dimensionless spreading coefficient. In the limit where all  $\mu_i$  possess similar values, the circular segment shape minimizes the total energy compared to those for all other droplet shapes of similar size. For a quasi-2D system, such as a molecularly thin film, the circular segment approximation still describes the physical properties qualitatively correctly as long as the dipole moment densities of the phases do not differ much. Restricting ourselves to circular segment shapes and in the limit  $\Delta \rightarrow 0$ , we obtain the free energy (Appendices a–d)

$$F = \tilde{F} + 2R\lambda_{12} \left\{ \alpha \left( 1 - 2 \frac{(\mu_1 - \mu_2)(\mu_3 - \mu_2)}{\lambda_{12}} \cos(\alpha) - \frac{(\mu_1 - \mu_2)^2}{\lambda_{12}} \ln \frac{8R}{\Delta e} \right) + \sin \alpha \left( -(S + 1) + \frac{(\mu_1 - \mu_2)(\mu_3 - \mu_2)}{\lambda_{12}} \ln \frac{4R^2 \sin^4(\alpha)}{\Delta^2} - \frac{(\mu_1 - \mu_2)^2}{\lambda_{12}} \ln \frac{8R \sin^3(\alpha/2)}{\Delta \cos(\alpha/2)} \right) - \frac{(\mu_1 - \mu_2)^2}{\lambda_{12}} \text{Im}[\text{dilog}(1 + e^{i\alpha}) - \text{dilog}(1 - e^{i\alpha})] \right\} \quad (4)$$

with

$$R = \sqrt{\frac{A}{\left(\alpha - \frac{1}{2} \sin(2\alpha)\right)}} \quad (5)$$

the radius of curvature of the circular segment. In the general case instead of eq 2 the equilibrium contact angle is given by the solution of

$$\frac{\partial F}{\partial \alpha_A} = 0 \quad (6)$$

We have solved eq 6 numerically using the circular segment approximation (eq 4). Figure 1 shows results for the equilibrium contact angle at an indifferent support ( $S = -1$ ) as a function of the control parameter,  $\mu^2/\lambda_{12}$ ,<sup>5</sup> for  $\mu_1 = \mu_2 \pm \mu$ ,  $\mu_3 = \mu_2 \pm \beta\mu$  for (a)  $\beta = 0$ , (b)  $\beta = 1$ , and (c)  $\beta = 0.48$ . Note that both signs of the excess dipole moment density  $\mu$  lead to the same results because of the dependence of the control parameter on  $\mu^2$ . For  $\mu_1 \neq \mu_2 = \mu_3$  (case a), we find one minimum for the droplet shape at a distinct contact angle  $\alpha$ . For  $\mu \rightarrow 0$  the system behaves as in the 3D case and the droplet partially wets phase 3 given that  $-2 < S < 0$  with a contact angle given by Young's equation (eq 2). As  $\mu$  increases in the quasi-2D system, electrostatic repulsion between neighboring dipoles within the droplet increases their average distance. The model predicts that this may be achieved by spreading of the droplet at the 2,3 boundary. We find one energy minimum at  $\alpha = \alpha_w$ . The value of  $\alpha_w$  is generally smaller than that

obtained from Young's equation. For  $\mu^2/\lambda_{12} \gg 0$ , it approaches complete wetting ( $\alpha \approx \Delta^2/A$ ) exponentially as

$$\alpha_w \left( \mu^2/\lambda_{12} > -S/(1-\beta) \ln \frac{3\pi A}{e^4 \Delta^2} \right) \rightarrow \frac{e^4 \Delta^2}{6A} \exp \left[ \frac{S\lambda_{12}}{(\mu_1 - \mu_3)(\mu_2 - \mu_1)} \right] \text{ for } \frac{\mu_3 - \mu_2}{\mu_1 - \mu_2} < 1 \quad (7)$$

Upon increasing  $\mu$  or  $A$  even further, the *shape* of the droplets in the bulk changes from circular to ellipsoidal at  $\mu^2/\lambda_{12} \ln(8A^{1/2}/\pi^{1/2}e^{7/3}\Delta) > 1$ ;<sup>14</sup> elongation proceeds until phase 1 finally forms a labyrinth pattern within phase 2.

A different situation occurs when  $\mu_2 \neq \mu_1 = \mu_3$  (case b). Apart from repulsion between dipoles within the droplet, there is an additional repulsive interaction between the dipoles in the droplet and those in phase 3. This promotes dewetting of the droplet from the 2,3 interface (Figure 1). Upon increasing  $\mu^2/\lambda_{12}$  or  $A$ , the droplet completely dewets ( $\alpha \approx \pi - (\Delta/A^{1/2})^{1/2}$ ) the 2,3 boundary. For large  $\mu^2/\lambda_{12}$  the energy minimum at  $\alpha_{dw}$  is described by

$$\alpha_{dw} \left( \mu^2/\lambda_{12} > \frac{S+2}{16\beta} \ln \frac{\pi^3 e^6 A}{4\Delta^2} \right) \rightarrow \pi - \frac{\Delta^{1/2} \pi^{1/4}}{\sqrt{2} e^{3/2} A^{1/4}} \exp \left[ \frac{(S+2)\lambda_{12}}{4(\mu_1 - \mu_2)(\mu_3 - \mu_2)} \right] \text{ for } (\mu_1 - \mu_2)(\mu_3 - \mu_2) > 0 \quad (8)$$

and exponentially approaches complete dewetting.

If the dipole densities of the phases are such that the droplet is repelled from the 2,3 boundary, that is,  $\text{sign}(\mu_3 - \mu_2) = \text{sign}(\mu_1 - \mu_2)$ , and if  $|\mu_3 - \mu_2| < |\mu_1 - \mu_2|$  (case c), we find one equilibrium contact angle for  $\mu^2/\lambda_{12} < [\mu^2/\lambda_{12}]_c$ , described by eq 2 when  $\mu \rightarrow 0$ , and two energy minima for  $\mu^2/\lambda_{12} > [\mu^2/\lambda_{12}]_c$ . The minima are given by eqs 7 and 8 if  $\mu^2/\lambda_{12}$  is large. In Figure 1 this is illustrated for the special case  $(\mu_3 - \mu_2) = 0.48(\mu_1 - \mu_2)$ , for which the transition is of second order. For large  $\mu^2/\lambda_{12}$  the minimum at  $\alpha_{dw}$  is metastable, while that at  $\alpha_w$  is stable. For  $(\mu_3 - \mu_2) \neq 0.48(\mu_1 - \mu_2)$ , the transition is of first order with a jump of the minimum contact angle at the transition. The contact angle transition occurs at  $[\mu^2/\lambda_{12}]_c$ , which is larger than the critical value  $[\mu^2/\lambda_{12}]_s$ , where the shape transitions occur in the bulk (shaded region in Figure 1).

### Experimental Observations

We have tested the predictions of the model experimentally in Langmuir monolayers of methyloctadecanoate in the quasi-2D liquid crystalline (LC)/liquid expanded (LE)/gaseous (G) three-phase coexistence region<sup>15</sup> using fluorescence microscopy.<sup>12</sup> Methyl octadecanoate (Aldrich), labeled with (1% 4-hexadecylamino-7-nitrobenz-2-oxa-1,3-diazole, Molecular Probes) was spread on pure water (Millipore Milli Q at 18 M $\Omega$  cm) without further purification on a home-built trough described in detail elsewhere.<sup>16</sup> The fluorescence microscope images were videotaped and later digitized. Contact angles at the three-phase intersections were measured by attaching tangent lines to each individual image via eye inspection. Angles between those tangents were determined using image analysis software (Adobe photoshop). Compression or expansion of the monolayer changes the relative areas of the three distinct phases within the surface

(14) Lee, K. Y. C.; McConnell, H. M. *J. Phys. Chem.* **1993**, *97*, 9532–9539.

(15) The three-phase coexistence region is found experimentally in a temperature range spanning 10 K. This is in contrast to the Gibbs phase rule, which applies for macroscopically separated phases.

(16) Wurlitzer, S.; Lautz, C.; Liley, M.; Duschl, C.; Fischer, Th. M. *J. Phys. Chem. B* **2001**, *105*, 182–187.

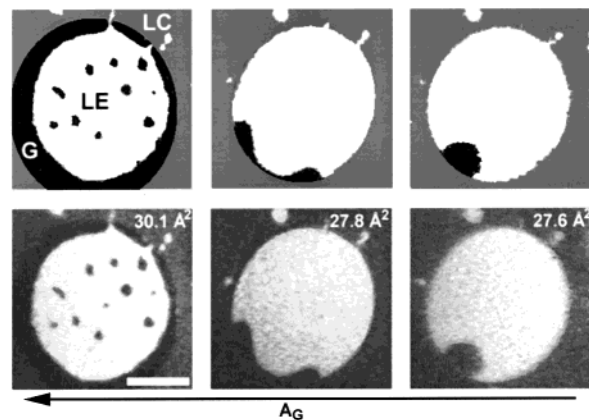


**Figure 2.** Experimental observation of a partial/complete wetting transition in an octadecanoate Langmuir monolayer using fluorescence microscopy (1 mol % NDB-HDA,  $T \approx 23$  °C). Values of the molecular area,  $a$ , per molecule are given in the panels. At  $a = 30.1$  Å<sup>2</sup>, a large gas bubble (dark) completely wets the LC (gray)/LE (bright) interface. Smaller gas bubbles within the LE phase are close to the shape instability, such that elongated and circular shapes coexist. Upon compression, the gas bubbles in the interior become circular, and then disappear, and finally the gas partially dewets the LC–LE interface ( $a = 27.8$  and  $27.6$  Å<sup>2</sup>). For a clear identification of the phases, we have posed manipulated images above their originals, where the different phases have been marked in black, gray, and white. The scale bar is  $25 \mu\text{m}$ .

film, enabling a controlled change of the droplet area  $A$ . In contrast to the theoretical calculations, all phase boundaries are usually curved, such that two of the three phases consist of droplets of finite area. In such a situation, the phase with the smaller area should be identified as phase 1 of the theoretical model. Compression also affects the parameter  $\mu^2/\lambda_{12}$ , since the concentration of the admixed fluorescent probe, enriched in the LE phase and known to reduce  $\lambda_{LE/G}$ , is proportional to the inverse of the relative area fraction of this phase. For this system  $\mu_G \approx 0$ ,  $\mu_{LC} \approx 0.49$  (pN)<sup>1/2</sup>,  $\mu_{LE} \approx 0.25$  (pN)<sup>1/2</sup>,  $0.2 < \lambda_{LE/G} < 0.5$  pN,<sup>18</sup> and the cutoff parameter is of the order  $\Delta \approx 0.6$  nm.<sup>5</sup> Figure 2 shows the behavior of the gas phase, to be identified with phase 1 in Figure 1, which wets completely the circular LE/LC boundary before the surface film is compressed from an initial area per molecule,  $a = 30.1$  Å<sup>2</sup> at  $T = 23 (\pm 0.3)$  °C.<sup>19</sup> Since  $\mu_G < \mu_{LE}$ ,  $\mu_{LC}$ , the excess dipole moment density  $\mu$  is negative in this case. At  $a \approx 30$  Å<sup>2</sup>, the monolayer is close to the bulk shape instability (shaded region in Figure 1), and as a consequence, gas bubbles observed within the LE phase show a coexistence of circular and elongated shapes. Upon compression, all gas bubbles within the LE phase become circular while concurrently the area  $A$  of the gas phase decreases. Eventually (Figure 2,  $a = 27.8$ – $27.6$  Å<sup>2</sup>), the gas phase is driven across the wetting instability, which leads to progressive partial dewetting of the LC/LE boundary. This observation is consistent with the behavior predicted by the model for  $\mu_G < \mu_{LE}$ ,  $\mu_{LC}$ . Figure 3 shows observations on LE droplets at the LC/G boundary line at  $T = 24 (\pm 0.3)$  °C. From the observed phase morphology, LE has to be identified with phase 1 of the theoretical model. In this situation, compression of the monolayer ( $a = 26.2 \rightarrow 24.5$  Å<sup>2</sup>) increases the size,  $A_{LE}$ , and concurrently affects  $\mu^2/\lambda_{LE/G}$  via the probe concentration within the LE droplets. As a consequence, the length of the contact line between the LE droplet and the LC phase decreases until the LE droplet finally dewets the LC/G boundary at  $24.5$  Å<sup>2</sup>, consistent with the scenario predicted by the model for case b.

In all experimental systems one finds  $|\mu_{LC} - \mu_G| > |\mu_{LE} - \mu_G|$  such that one does not encounter the situation described by case c. One may, however, study this case experimentally in a situation

(17) Heinig, P.; Wurlitzer, S.; Steffen, P.; Kremer, F.; Fischer, Th. M. *Langmuir* **2000**, *16*, 10254.

(18) Wurlitzer, S.; Steffen, P.; Fischer, Th. M. *J. Chem. Phys.* **2000**, *112*, 5915–5918.

(19) Khattari, Z.; Fischer, Th. M. Shapes of Langmuir Monolayer Domains in Confined Geometries. *J. Phys. Chem. B.*, in press.

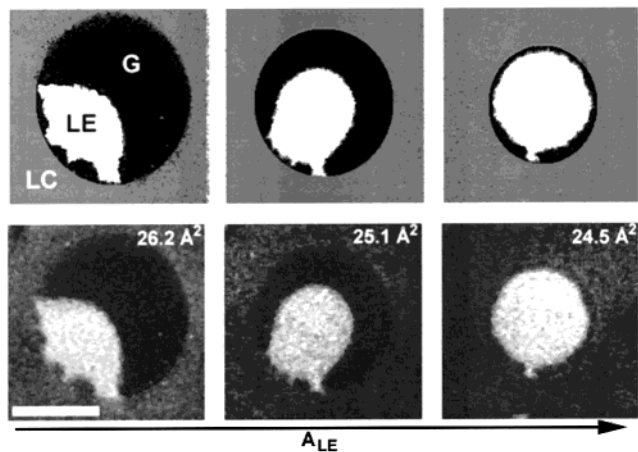


**Figure 3.** Partial wetting/dewetting transition of a LE droplet (bright) from the G (dark)–LC (gray) boundary. Upon compression, the area of the LE phase and its contact angle at the LC phase increase ( $a = 26.2$  and  $25.1 \text{ \AA}^2$ ) until the droplet dewets completely from the G–LC boundary ( $24.5 \text{ \AA}^2$ ). The small connection of the LE droplet to the LC phase in the final stage is also an electrostatic effect, understood when going beyond the circular segment approximation. It is eventually disconnected from the LC boundary on further compression, when concurrently the thickness of the G phase is shrinking to the resolution limit of the microscope. For a clear identification of the phases, we have posed manipulated images above their originals, where the different phases have been marked in black, gray, and white. The scale bar is  $25 \mu\text{m}$ .

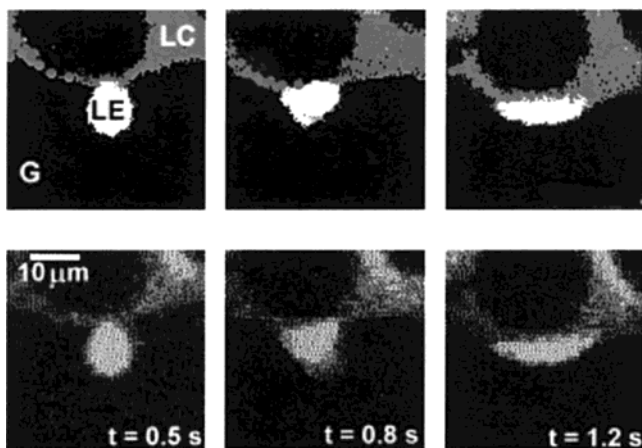


**Figure 4.** Discontinuous transition of the contact angle of a LE droplet (bright) partially wetting a thin stripe of the LC phase (gray). The droplet was created by cutting a LE lamella connecting two LC–G boundaries within a G cavity using a focused laser beam. The LE lamella shortens and forms the partially dewetting droplet shown at  $t = 0.5$  s. The droplet remains at a contact angle of  $\alpha_{\text{dw}} \approx 100^\circ$  for  $0.5$  s (metastable state) and then jumps to a contact angle of  $\alpha_{\text{w}} \approx 30^\circ$  (stable partial wetting state) within  $0.1$  s. The time reading refers to the abscissa of Figure 5. For a clear identification of the phases, we have posed manipulated images above their originals, where the different phases have been marked in black, gray, and white. The scale bar is  $10 \mu\text{m}$ .

where an LE droplet is associated with a thin LC lamella that may be found by studying a 2D LC/G foamlike structure. In such a situation,  $|\mu_2 - \mu_3|$  is effectively reduced, since  $\mu_{\text{LCG}}^{\text{foam}} \ll \mu_{\text{LC}}$  and a 2D LC/G foam mimics an extended solid phase of low dipole density. An experimental realization and its dynamic development are shown in Figure 4. A LE droplet (bright) partially wets a thin stripe of the LC phase (gray). Initially it partially wets the LC/G interface with a contact angle of  $\alpha_{\text{dw}} \approx 100^\circ$ , and remains at this contact angle for  $\sim 0.5$  s. At  $t \sim 0.8$  s, it jumps to a lower contact angle,  $\alpha_{\text{w}} \approx 30^\circ$ , within a tenth of a second, where it then remains stable. The contact angle dynamics of the droplet of

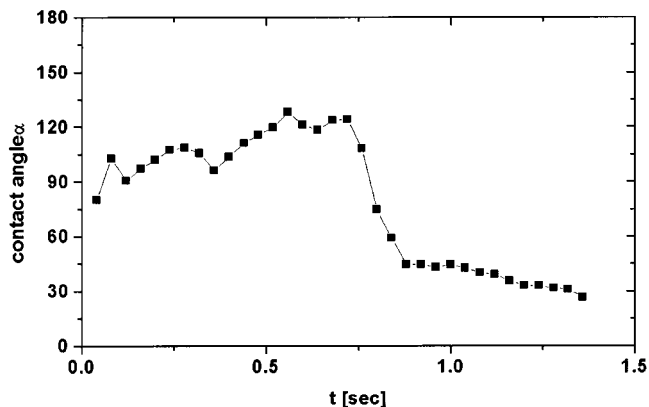


**Figure 5.** Contact angle dynamics of the LE droplet in Figure 4, determined by image analysis of consecutive digitized fluorescence microscopy images, showing the metastability (stability) of the initial (final) contact angle.

Figure 4, taken from consecutive digitized images, is depicted in Figure 5. The observed scenario agrees with predictions derived for case c: Initially the state of the droplet is described by the metastable branch with a contact angle  $\alpha_{\text{dw}}$ ; it remains there for a while until it jumps to the stable situation characterized by  $\alpha_{\text{w}}$ .

### Discussion

The main effect of the electrostatic interactions is to elongate the droplet either parallel or perpendicular to the interface, as has been derived for flat solid boundaries in the theoretical section. In the experiments, however, also the liquid condensed boundary is curved. As long as the curvature of the droplet is much larger than that of the LC boundary, little effect is expected from the additional curvature of the LC boundary. However, when the droplet curvature comes into the same order of magnitude as that of the LC boundary, which happens when the partially wetting droplet approaches either complete wetting or complete dewetting, then the electrostatic interactions will act to reduce the tendency to completely wet or dewet the LC boundary. In the wetting case, the droplet ends—being far apart if the boundary is flat—reapproach if the boundary is curved and electrostatically repel each other. The points in the left-hand micrograph ( $a = 30.1 \text{ \AA}^2$ ) of Figure 2 at which the LE phase “pokes through” to the LC phase presumably occur because of such dipole–dipole interactions between the ends of the gas bubble. If the LC phase is curved in the dewetting case, the LC wall opposite the base of the partially dewetting LE domain exhibits an electrostatic force on the LE domain in the direction of its base, which exactly cancels the force originating from the LC phase near the base, if the droplet is centered within the cavity. Hence, the tendency for complete dewetting is also suppressed by the LC curvature.

Compression of the monolayer does not only change the area of the partially wetting droplet phase but also significantly reduces the radius of the LC boundary ( $dR/R \approx 1/2$ ), and the Laplace pressure inside the cavity may change by the order ( $dR\lambda_{\text{LC}}/R^2 \approx 10^{-7} \text{ N/m}$ ). Such pressure changes are weak compared to the elasticity  $E = -\Gamma d\sigma/d\Gamma$  ( $\Gamma$  is the surface concentration, and  $\sigma$  is the surface tension) of the LE phase but might cause some compression of the gaseous phase. Compression of the gaseous phase could result in an increased dipole density of the gaseous phase, that is, a decrease of the dipole density difference to those of the LC and the LE phases. Experiments on shape instabilities in LC cavities seem to support such effects.<sup>19</sup> Again this effect of curvature should counteract a complete wetting and dewetting.

Finally, describing the shape of droplets as circular segments is an approximation which becomes exact as  $\mu \rightarrow 0$ . The larger  $\mu$ , the more deviations from the circular segment shape will play a role. This will be most pronounced when  $\beta \neq 0$  and the droplet is repelled from its support.<sup>20</sup>

The observed dependence of the wetting properties between 2D phases on both dipolar densities, and hence the membrane potential, and the lateral morphology should bear significant implications for the reactivity between interacting protein species associated with distinct coexisting phases. It has been shown<sup>21</sup> that the difference in lipid composition of the cytosolic and luminal leaflets of the plasma membrane of polarized cells gives rise to dipole moment densities similar to those observed in Langmuir monolayers. While the membrane may be homogeneous on the micron scale, domains of different phases have been reported on the nanoscale in epithelial cells,<sup>11</sup> which is also the length scale where electrostatic interactions are screened at physiological salt concentrations. This length scale would indicate that the line tensions between these phases are only a factor of  $\sim 5$  smaller than those reported here. Many biomembrane reactions result in large changes in membrane potential.<sup>22–27</sup> If a protein that is preferentially dissolved in one particular phase within the membrane reacts with an inhibitor (activator) which is in turn preferentially dissolved in a distinct coexisting phase, the activity of such a protein will strongly depend on the wetting behavior between the coexisting phases. The only region where activation or inhibition of the protein is possible is in the vicinity of the contact line between the two phases. If the boundary between both phases is wetted completely by the third phase, no inhibition or activation of the protein is possible. A change in membrane potential of one of the phases, triggered for example by active transport through an ion channel, could alter the dipole density differences between the phases such that a transition toward partial wetting occurs, bringing the phases harboring the protein and its inhibitor (activator) into contact. Opposite effects might occur, if the growth of a domain of one of the phases is fed by material transport from a second partially wetting phase. As the domain of the first phase grows, dewetting of the second phase could be caused by the increase in area of the domain, thereby cutting its routes of supply as well as the possibility of interaction between species within the first phase and in the second phase. The heterogeneity of the lipid environment and the sensitivity of the lateral phase structure to the sizes and surface potentials of individual lipid domains would in this case represent an important factor that controls the activation or deactivation of a particular protein function. Hence, a lipid bilayer would not only provide the proper environment for the spatial organization of membrane proteins but also control their activity by a mechanism that bears its origin entirely in the dimensionality and asymmetry of the system.

(20) Heinig, P.; Steffen, P.; Wurlitzer, S.; Fischer, Th. M. *Langmuir* (in press).

(21) Brockman, H. *Chem. Phys. Lipids* **1994**, *73*, 57–79.

(22) Elston, T.; Wang, H.; Oster, G. *Nature* **1998**, *391*, 510–513.

(23) Steinberg-Yfrach, G.; Rigaud, J. L.; Durantini, E. N.; Moore, A. L.; Gust, D.; Moore, T. A. *Nature* **1998**, *392*, 479–482.

(24) Rastogi, V. K.; Girvin, M. E. *Nature* **1999**, *402*, 263–268.

(25) Sansom, M. S. P. *Prog. Biophys. Mol. Biol.* **1991**, *55*, 139–235.

(26) Sunshine, C.; McNamee, M. G. *Biochim. Biophys. Acta* **1994**, *1191*, 59–64.

(27) Baenziger, J. E.; Morris, M. L.; Darsaut, T. E.; Ryan, S. E. *J. Biol. Chem.* **2000**, *275*, 777–784.

**Acknowledgment.** We thank H. Mohwald for generous support and stimulating discussions. This work was supported by the Deutsche Forschungsgemeinschaft (DFG) with a Heisenberg fellowship to T.M.F., and further within the priority program “Wetting and structure formation at interfaces” (Fi 548/4-1 and Lo352/7-2) and the SFB 294, TP F3.

### Appendix A: Evaluation of the Dipolar Energy of a Liquid 2D Circular Segment Droplet Wetting a Straight Gas–Solid Boundary Line

An analytical calculation of the electrostatic energy of a sessile droplet with a phase boundary shaped like a circular cap is performed in this appendix. One may then write the total energy of the system as a sum of line energies and electrostatic energies:

$$F = \sum_{i,j} F_{\text{el}}^{ij} + F_{\lambda} \quad (\text{A.1})$$

The two types of energies are<sup>5,28</sup>

$$F_{\text{el}}^{ij} = \frac{\mu_i \mu_j}{2} \int_{A_i} \int_{A_j} \frac{dA_i dA_j}{((\mathbf{r} - \mathbf{r}')^2 + \Delta^2)^{3/2}} \stackrel{i=j}{=} A_i \epsilon_i - \frac{\mu_i^2}{2} \oint \frac{ds \cdot ds'}{\sqrt{(\mathbf{r} - \mathbf{r}')^2 + \Delta^2}} - \mu_i^2 \oint ds \quad (\text{A.2})$$

and

$$F_{\lambda} = \lambda_{12}[-(S+1)B + C] \quad (\text{A.3})$$

Here,  $A_i$  and  $A_j$  are two areas,  $ds$  and  $ds'$  are line elements attached to them, and  $\Delta$  is a cutoff length below which the dipole forces are screened by other interactions within the monolayer. The dipole density difference  $\mu_i$  is proportional to the difference in surface potential between the interior and the exterior of the droplet,<sup>28</sup>  $\Delta V_i - \Delta V_g$ .

$$\mu_i = \sqrt{\frac{\epsilon_0}{4\pi} \frac{2\epsilon_w \epsilon_{\text{air}}}{(\epsilon_{\text{air}} + \epsilon_w)}} (\Delta V_i - \Delta V_g) \quad (\text{A.4})$$

If one calculates the electrostatic energy of one area  $A$  (i.e.,  $i = j$ ), the double integral over the droplet area can be replaced by a double integral over its perimeter. Also, the electrostatic repulsion renormalizes the line tension.<sup>28,29</sup> For the explicit geometry depicted in Figure 1, the symbol  $B$  denotes the base of the droplet, that is, the length of the solid–liquid interface, while  $C$  denotes the length of the droplet cap, that is, the length of the gas–liquid interface.

In the following calculations, the approximation of the shape by a circular segment will be used as a model, and one finds

$$B = 2R \sin \alpha$$

$$C = 2R\alpha \quad (\text{A.5})$$

where  $\alpha$  is the contact angle. The radius of curvature  $R$  of the segment is given by eq 5. The circular-cap shape can be described mathematically by the following equation:

(28) Riviere, S.; Henon, S.; Meunier, J.; Albrecht, G.; Boissonnade, M. M.; Baszkin, A. *Phys. Rev. Lett.* **1995**, *75*, 2506–2510.

(29) McConnell, H. M.; de Koker, R. *J. Phys. Chem.* **1992**, *96*, 7101–7103.

$$\begin{aligned} y^2 + (x + R \cos \alpha)^2 &= R^2 & \text{for } 0 < x < R(1 - \cos \alpha) \\ x = 0 & & \text{for } |y| < R \sin \alpha \end{aligned} \quad (\text{A.6})$$

Shape dependent terms in the energy in eq A.2 only depend on dipole density differences between the phases. By choosing phase 2 as the reference phase, only the energies  $F_{\text{el}}^{11}$ ,  $F_{\text{el}}^{13} = F_{\text{el}}^{31}$ , and  $F_{\text{el}}^{33}$  differ from zero.  $F_{\text{el}}^{33}$  does not depend on the droplet shape and is of no interest when determining equilibrium contact angles. We are left with the calculation of  $F_{\text{el}}^{11}$  and  $F_{\text{el}}^{13}$ , which is done in Appendices B and C.

### Appendix B: Electrostatic Self Energy of the Droplet

The dipole–dipole electrostatic self energy of a droplet is given by the expression

$$\begin{aligned} F_{\text{el}}^{11} &= A_1 \epsilon_1 - \frac{1}{2} (\mu_1 - \mu_2)^2 \int_{-\pi}^{\pi} \int_{-\pi}^{\pi} \frac{\mathbf{ds}_1(\varphi_1) \cdot \mathbf{ds}_2(\varphi_2)}{\sqrt{r_1^2 + r_2^2 - 2r_1 r_2 \cos(\varphi_1 - \varphi_2) + \Delta^2}} - \\ &(\mu_1 - \mu_2)^2 (B + C) = A_1 \epsilon_1 - \frac{1}{2} (\mu_1 - \mu_2)^2 (I_{\text{BB}} + I_{\text{CC}} + \\ &2I_{\text{CB}}) - (\mu_1 - \mu_2)^2 (B + C) \end{aligned} \quad (\text{B.1})$$

where  $r_i = r(\varphi_i)$  is a description of the droplet boundary in polar coordinates and  $\epsilon_1$  is a shape independent energy density. The cutoff  $\Delta$  has been introduced to prevent divergence of the dipolar energy  $F_{\text{el}}^{11}$ .  $\Delta$  is assumed to be very small in the following calculations. We split the double line integrals in eq B.1 into integrals along the base B and cap C of the wetting droplet. We then find

$$\begin{aligned} I_{\text{BB}} &= \int_{-B/2}^{B/2} \int_{-B/2}^{B/2} \frac{dy dy'}{\sqrt{(y - y')^2 + \Delta^2}} \xrightarrow{\Delta \rightarrow 0} 2B \ln \left( \frac{2B}{\Delta e} \right) \\ &= 4R \sin(\alpha) \ln \left( \frac{8R \sin(\alpha/2) \cos(\alpha/2)}{\Delta e} \right) \end{aligned} \quad (\text{B.2})$$

$$I_{\text{CC}} = R \int_{-\alpha}^{\alpha} \int_{-\alpha}^{\alpha} d\varphi_1 d\varphi_2 \frac{\cos(\varphi_1 - \varphi_2)}{\sqrt{4 \sin^2 \left( \frac{\varphi_1 - \varphi_2}{2} \right) + \left( \frac{\Delta}{R} \right)^2}} \quad (\text{B.3})$$

The above integral depends only on the angle difference  $\varphi_1 - \varphi_2$ , and by substituting  $\psi = (\varphi_1 + \varphi_2)/2$  and  $\vartheta = \varphi_1 - \varphi_2$  in the above equation, we obtain

$$I_{\text{CC}} = 4R \int_0^{2\alpha} d\vartheta (\alpha - \vartheta/2) \frac{1 - 2 \sin^2(\vartheta/2)}{\sqrt{4 \sin^2(\vartheta/2) + (\Delta/R)^2}} \quad (\text{B.4})$$

Since  $\Delta$  is small, we may retain only first-order terms in  $\Delta$  to find<sup>29</sup>

$$I_{\text{CC}} = 8R \sin(\alpha) + 4R\alpha \ln \left( \frac{8R \tan(\alpha/2)}{\Delta e^2} \right) - R \int_0^{2\alpha} d\vartheta \frac{\vartheta}{\sin(\vartheta/2)} \quad (\text{B.5})$$

Integrating the last term by parts results in

$$\begin{aligned} I_{\text{CC}} &= 8R \sin(\alpha) + 4R\alpha \ln \left( \frac{8R \tan(\alpha/2)}{\Delta e^2} \right) - \\ &4R\alpha \ln(\tan(\alpha/2)) + 2R \int_0^{2\alpha} d\vartheta \ln(\tan(\vartheta/4)) \end{aligned} \quad (\text{B.6})$$

The remaining integral can be evaluated by noting that

$$\int_0^{2\alpha} d\vartheta \ln(\tan(\vartheta/4)) = \text{Im} \int_0^{2\alpha} d\vartheta \ln \left( \frac{1 - e^{i\vartheta/2}}{1 + e^{i\vartheta/2}} \right) \quad (\text{B.7})$$

substituting  $z = 1 \mp e^{i\vartheta/2}$  in the numerator and denominator, respectively. Then eq B.7 becomes

$$\begin{aligned} \text{Im} \int_0^{2\alpha} d\vartheta \ln \left( \frac{1 - e^{i\vartheta/2}}{1 + e^{i\vartheta/2}} \right) &= \\ 2 \text{Im} \left\{ \int_1^{1-e^{i\alpha}} dz \frac{\ln(z)}{z-1} - \int_1^{1+e^{i\alpha}} dz \frac{\ln(z)}{z-1} \right\} \end{aligned} \quad (\text{B.8})$$

where  $\text{Im}$  is the imaginary part of the integral. Also, the integration over  $z$  has been split into two parts:  $\int_0^{1-e^{i\alpha}} \rightarrow \int_0^1 + \int_1^{1-e^{i\alpha}}$ . The imaginary part of the first integral evaluates to zero. Defining the dilogarithm function as<sup>30</sup>

$$\text{dilog}(\xi) = - \int_1^{\xi} dz \frac{\ln(z)}{z-1} \quad (\text{B.9})$$

where  $\xi$  is a complex number, we obtain

$$\begin{aligned} I_{\text{CC}} &= 8R \sin(\alpha) + 4R\alpha \ln \left( \frac{8R \tan(\alpha/2)}{\Delta e^2} \right) - \\ &4R\alpha \ln(\tan(\alpha/2)) + 4R \text{Im} \{ \text{dilog}(1 + e^{i\alpha}) - \\ &\text{dilog}(1 - e^{i\alpha}) \} \end{aligned} \quad (\text{B.10})$$

The last integral is

$$\begin{aligned} I_{\text{CB}} &= \int_{-\alpha}^{\alpha} d\varphi \int_{-B/2}^{B/2} dy \times \\ &\frac{-R \cos(\varphi)}{\sqrt{(y - R \sin(\varphi))^2 + (R \cos(\alpha) - R \cos(\varphi))^2 + \Delta^2}} \end{aligned} \quad (\text{B.11})$$

The integration over the variable  $y$  is straightforward. Utilizing trigonometric identities and arranging the terms, we obtain

$$\begin{aligned} I_{\text{CB}} &= R \int_{-\alpha}^{\alpha} d\varphi \cos(\varphi) \left\{ \ln \left( \tan \left( \frac{\alpha + \varphi}{4} \right) \right) + \right. \\ &\left. \ln \left( \tan \left( \frac{\alpha - \varphi}{4} \right) \right) \right\} = 2R \int_{-\alpha}^{\alpha} d\varphi \cos(\varphi) \ln \left( \tan \left( \frac{\alpha + \varphi}{4} \right) \right) \end{aligned} \quad (\text{B.12})$$

where, in the last step, a substitution of  $\varphi \rightarrow -\varphi$  in the second integrand has been used. The remaining integral can be calculated by integration by parts. One finds

$$I_{\text{CB}} = 4R \sin(\alpha) \ln(\tan(\alpha/2)) - 4R \sin(\alpha) \quad (\text{B.13})$$

Finally, substituting eqs B.2, B.10, and B.13 into eq B.1 and using

(30) Abramowitz, M.; Stegun, I. A. *Pocketbook of mathematical functions*; Verlag Harri Deutsch Thun: Frankfurt, 1984; p 448.

$$-(\mu_1 - \mu_2)^2 \oint ds = -(\mu_1 - \mu_2)^2 (B + C) = -2R(\mu_1 - \mu_2)^2 (\alpha + \sin(\alpha))$$

one finds

$$F_{el}^{11} = A_1 \epsilon_1 - 2R(\mu_1 - \mu_2)^2 \left\{ \alpha \ln \frac{8R}{\Delta e} + \sin \alpha \ln \frac{8R \sin^3 \alpha/2}{\Delta \cos \alpha/2} + \text{Im}[\text{dilog}(1 + e^{i\alpha}) - \text{dilog}(1 - e^{i\alpha})] \right\} \quad (\text{B.14})$$

### Appendix C: Wall Droplet Energy

The interaction energy between the droplet and the wall can be written as

$$F_{el}^{12} + F_{el}^{21} = (\mu_3 - \mu_2)(\mu_1 - \mu_2) I_{dw} \quad (\text{C.1})$$

where

$$I_{dw} = \int_0^{R(1-\cos(\alpha))} dx \int_{-F(x)}^{F(x)} dy \int_{-\infty}^0 dx' \int_{-\infty}^{\infty} dy' \times \frac{1}{[(x-x')^2 + (y-y')^2 + \Delta^2]^{3/2}} \quad (\text{C.2})$$

$$\text{with } F(x) = \sqrt{R^2 - (x + R \cos(\alpha))^2}$$

The integration over the variables  $y'$ ,  $x'$ , and  $y$  is straightforward and yields

$$I_{dw} = 2 \int_0^{R(1-\cos(\alpha))} \frac{(\pi - 2 \arctan(x/\Delta))}{\Delta \sqrt{R^2 - (x + R \cos(\alpha))^2}} dx \quad (\text{C.3})$$

One can rewrite this integral by adding and subtracting counter terms as follows:

$$I_{dw} = 2 \int_0^{R(1-\cos(\alpha))} \frac{(\pi - 2 \arctan(x/\Delta))}{\Delta} \times [\sqrt{R^2 - (x + R \cos(\alpha))^2} - R \sin(\alpha)] dx + 2R \sin(\alpha) \int_0^{R(1-\cos(\alpha))} \frac{(\pi - 2 \arctan(x/\Delta))}{\Delta} dx \quad (\text{C.4})$$

In the first term one may interchange the limit  $x \rightarrow 0$  with  $\Delta \rightarrow 0$ , while the latter integral may be performed for

finite  $\Delta$  and the limit  $\Delta \rightarrow 0$  is performed after the integration. One finds

$$I_{dw} = \int_0^{R(1-\cos(\alpha))} \frac{4}{x} [\sqrt{R^2 - (x + R \cos(\alpha))^2} - R \sin(\alpha)] dx + 4R \sin(\alpha) \ln \left( \frac{R(1 - \cos(\alpha))e}{\Delta} \right) \quad (\text{C.5})$$

The integral in eq C.5 is standard, and finally, one finds

$$I_{dw} = 4R \left[ -\alpha \cos(\alpha) + \sin(\alpha) \ln \left( \frac{2R \sin^2 \alpha}{\Delta} \right) \right] \quad (\text{C.6})$$

### Appendix D: Total Droplet Energy

Using eqs C.1, B.14, A.3, and A.5 yields the total droplet energy in eq 4, where terms which do not depend on the contact angle have been absorbed in the constant  $\tilde{F}$ . For  $\alpha \approx 0$ , eq 4 may be simplified using eq 5 to yield

$$F(\alpha \rightarrow 0) = \tilde{F} + \sqrt{6A}(\mu_1 - \mu_2)(\mu_3 - \mu_1)\alpha^{-1/2} \times \ln \left( \alpha \frac{6A}{e^2 \Delta^2} \exp \left[ \frac{-S \lambda_{12}}{(\mu_1 - \mu_2)(\mu_3 - \mu_1)} \right] \right) \quad (\text{D.1})$$

The free energy diverges as  $\alpha \rightarrow 0$ , since the length of the base B of the wetting droplet diverges and the gain (loss) in free energy per unit length of the wetted interface is finite in the absence of dipolar contributions and also diverges logarithmically with the length of the base in the presence of dipolar interactions. Similarly, for  $\alpha \rightarrow \pi$  one finds

$$F(\alpha \rightarrow \pi) = F(\pi) + 8\sqrt{A/\pi}(\mu_1 - \mu_2)(\mu_3 - \mu_2)(\pi - \alpha) \times \ln \left( (\pi - \alpha) \sqrt{\frac{2\sqrt{A/\pi}}{e\Delta}} \exp \left[ \frac{-(S+2)\lambda_{12}}{4(\mu_1 - \mu_2)(\mu_3 - \mu_2)} \right] \right) \quad (\text{D.2})$$

The asymptotic expressions D.1 and D.2 both have one single extremum described by eqs 1 and 2. The extrema are minima if  $(\mu_3 - \mu_2)/(\mu_1 - \mu_2) < 1$  and if  $(\mu_1 - \mu_2)(\mu_3 - \mu_2) > 0$ , respectively. If the dipole differences between the phases are large compared to  $\lambda_{12}$ , then one finds that  $\alpha_w \approx 0$  and  $\alpha_{dw} \approx \pi$ , respectively, hold, such that the approximations in eqs D.1 and D.2 are justified a posteriori. In the opposite case, the full energy (eq 4) must be used to find the minima, which in this work has been done numerically.

LA011520Q